Journal of the Indian Chemical Society 102 (2025) 102251

Contents lists available at ScienceDirect

Journal of the Indian Chemical Society

journal homepage: www.journals.elsevier.com/journal-of-the-indian-chemical-society

# Study on the dechlorination kinetics of 2,3,3′-trichlorobiphenyl in transformer oil by electron beam irradiation

Hoang Trung Thong [a,b], Phan Dinh Tuan [a,b], Hai D. Tran [a,*], Phan Dinh Dong [a,b], Dinh Thi Nga [b,c], Trinh Van Tuyen [d], Uyen P.N. Tran [e], Mai Thanh Tung [f], Dang Van Phu [g]

[a] Ho Chi Minh City University of Natural Resources and Environment, 236B Le Van Sy St., Tan Binh District, Ho Chi Minh City, 70000, Viet Nam
[b] Applied Research Institute of Natural Resources, Materials and Environment, 58/4 Tran Van Du, Tan Binh District, Ho Chi Minh City, 70000, Viet Nam
[c] Institute of Environmental Science, Engineering and Management, Industrial University of Ho Chi Minh City, 12 Nguyen Van Bao St., Go Vap District, Ho Chi Minh City, 70000, Viet Nam
[d] Graduate University of Science and Technology, 18 Hoang Quoc Viet St., Hanoi, 10000, Viet Nam
[e] Van Hien University, 665-667-669 Dien Bien Phu St., Ward 1, District 3, Ho Chi Minh City, 70000, Viet Nam
[f] Hanoi University of Science and Technology, 1 Dai Co Viet St., Hanoi, 10000, Viet Nam
[g] Research and Development Center for Radiation Technology, 202A Road 11, Linh Xuan Ward, Thu Duc Town, Ho Chi Minh City, 70000, Viet Nam

A B S T R A C T

Radiolytic dechlorination represents a promising approach for the effective detoxification of polychlorinated biphenyls (PCBs). In this study, the dechlorination of 2,3,3′-trichlorobiphenyl — a model compound for PCBs — was investigated in transformer oil using electron beam irradiation. Experimental results demonstrated that electron beam irradiation decreases the degree of chlorination per molecule in PCBs. A kinetic model based on a radical-mediated mechanism integrating the depth-dependent effects was developed to describe the dechlorination process. This model comprises a system of seven ordinary differential equations representing the time-dependent concentrations of PCBs and biphenyl. The model showed good agreement with experimental data, providing valuable insights into the rate constants governing the dechlorination pathway, and revealing concentration profiles as a function of sample depth and time. Additionally, the role of the electronic properties of PCBs in determining their dechlorination selectivity was elucidated.

## 1. Introduction

Polychlorinated biphenyls (PCBs) are chemically stable, highly resistant to degradation, and therefore persist for decades in soil, sediment, and water, where they bioaccumulate throughout the food chain [1,2]. Human exposure to PCBs is associated with endocrine disruption, reproductive toxicity, neurotoxicity, and carcinogenicity [3,4]. As a result, substantial research has focused on developing efficient methods to detoxify PCBs.

Historically, PCBs were added to transformer and capacitor oils due to their excellent dielectric strength and non-flammability [5]. An estimated 1.324 million tons of pure PCBs were produced worldwide from 1930 to 1993 [6]. Although most countries banned or severely restricted PCB manufacture and trade in the 1970s [2], PCB-containing equipment produced before these regulations took effect still exists [7,8]. End-of-life units, therefore, pose a major waste management challenge.

Several methods have been developed for the removal or destruction of PCBs in transformer oil, each with distinct advantages and limitations. Incineration at high temperatures is an effective option for complete oxidation of PCBs [9]. However, this method requires strict control to prevent the formation of highly toxic by-products such as dioxins and furans, and it is unsuitable for oil recovery [10]. Solvent extraction can separate PCBs from oil, allowing the recovered oil to be reused, but the extracted PCBs must subsequently undergo additional treatment [11]. Catalytic and biological degradation methods have also been investigated, though their efficiency is generally low in non-aqueous oil environments [12]. Despite its relatively high investment cost, irradiation represents a promising alternative for PCB destruction in oil because it requires no complex pretreatment or chemical additives, can be performed in closed systems under ambient conditions, and does not generate secondary toxic compounds like dioxins [13,14]. Furthermore, irradiation facilities can be shared with other commercial applications, including food preservation and sterilization, enhancing the economic feasibility of the technology.

Reducing the number of chlorine atoms in a PCB molecule has been recognized as a practical approach to lowering its toxicity [15–17]. Radiolysis has emerged as a promising method for the dechlorination of chlorinated organic compounds [18–20] and is considered a viable

* Corresponding author.
*E-mail address:* tdhai@hcmunre.edu.vn (H.D. Tran).

https://doi.org/10.1016/j.jics.2025.102251
Received 29 June 2025; Received in revised form 31 October 2025; Accepted 3 November 2025
Available online 5 November 2025

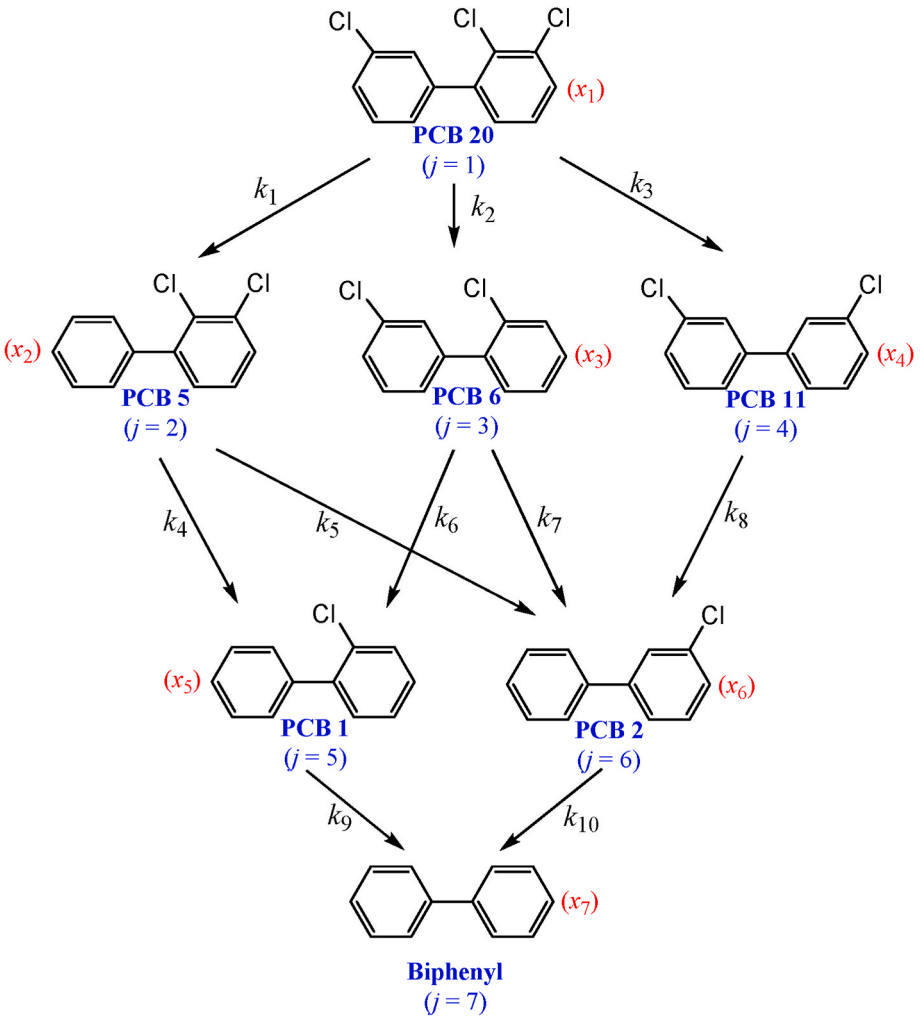


**Fig. 1.** Schematic diagram of the dechlorination pathway of PCB 20.

option for environmental remediation [21]. Chaychian et al. [22,23] successfully achieved complete dechlorination of 2,2′,6,6′-tetrachlorobiphenyl (PCB 54) in transformer oil using γ-irradiation while preserving oil quality, suggesting its potential for reuse. Under electron beam irradiation, Jung et al. demonstrated that PCBs in used transformer oil were completely decomposed, resulting in treated oil suitable for reuse as cutting oil or machine oil [13]. Compared with γ-irradiation, electron beam irradiation offers several advantages: (i) a much higher dose rate, (ii) the ability to be switched on and off instantly, (iii) the absence of radioactive materials, thereby avoiding source decay and hazardous waste disposal, and (iv) the capability to be adapted for continuous-flow treatment systems [24]. Owing to these advantageous features, electron beam irradiation represents a promising method for the destruction of PCBs in oils.

Under radiolytic conditions, dechlorination proceeds mainly via solvated electrons ($e^-_{sol}$), hydroxyl radicals ($HO^•$), and hydrogen radicals ($H^•$) [23,25]. The presence of precursor compounds that promote radical formation, such as KOH [25], 2-propanol [25–27], and methanol [28], has been shown to enhance the dechlorination efficiency significantly. Numerous studies have elucidated the mechanisms of PCB radiolytic dechlorination both in the presence and absence of additives [23,25,29–31]. However, in PCB-contaminated transformer oil, which consists primarily of hydrocarbons, solvated electrons and hydrogen radicals are considered the dominant reactive species responsible for cleaving C–Cl bonds [32]. Despite this, the dechlorination mechanism under direct electron beam irradiation has not been fully elucidated. Gaining a mechanistic understanding of PCB dechlorination is essential for predicting reaction pathways, optimizing processes, and designing effective remediation strategies.

The dechlorination kinetics of PCBs have been empirically examined in several previous studies [13,25,27]. In these reports, the second-order kinetic model was often adopted without detailed justification to describe the PCB dechlorination behavior [13,29,33]. This likely arises from applying the general reaction rate law to an elementary reaction between PCBs and reactive species such as solvated electrons or radicals. In principle, a kinetic model can be derived from the proposed reaction mechanism [34,35], thereby yielding dynamic parameters that provide valuable insights into the reaction process.

As reported in our previous study [36], 2,3,3′-trichlorobiphenyl (PCB 20) is the predominant congener present in used transformer oil, accounting for approximately 74 % of the total detected PCBs. This finding motivated the present study. The dechlorination pathway of model PCB 20 in transformer oil was proposed based on radical-mediated mechanisms. Furthermore, a depth dose distribution model was incorporated to explore its influence on the dechlorination kinetics of PCBs—an aspect that has been largely overlooked in previous research. The correlation between the electronic properties of PCBs and their susceptibility to dechlorination was also revealed.

## 2. Kinetic modeling of PCB dechlorination by electron beam irradiation

### 2.1. Proposed reaction mechanism

Upon electron beam irradiation, hydrocarbons (R–$CH_3$) in transformer oil initiates the random capture of incident electrons [37], promoting the molecules to an excited state, (R–$CH_3$)*. This state is ultrashort-lived (lifetime <100 ps) [38], as shown in Reaction (1). A significant fraction of these excited species then relaxes to the ground state, releasing the absorbed energy predominantly as heat, described by Reaction (2).

$$R-CH_3 + e^- \rightarrow (R-CH_3)^* \quad (1)$$

$$(R-CH_3)^* \rightarrow R-CH_3 + \text{heat} \quad (2)$$

Because C–H bonds cleave more readily than C–C bonds [32], the excited hydrocarbon molecules can undergo C–H bond cleavage to generate hydrogen radicals ($H^\bullet$) [39,40], as represented in Reaction (3). The generated $H^\bullet$ can rapidly and non-selectively react with neighboring species, including radicals, ions, and neutral molecules.

$$(R-CH_3)^* \rightleftharpoons R-CH_2^\cdot + H^\cdot \quad (3)$$

Owing to the presence of conjugated π-electrons, the benzene rings of PCBs can delocalize absorbed electrons and dissipate excitation energy by electronic relaxation [32]. Consequently, electron uptake principally produces excited PCB species ($Cl_p$–Bph)* rather than radical intermediates, as in Reaction (4). Electron absorption by the aromatic rings enhances the affinity of $H^\bullet$ for carbon atoms in PCB structures that possess low partial charges. Upon returning to the ground state, the excited PCBs release thermal energy, as shown in Reaction (5).

$$Cl_p - Bph + e^- \rightarrow (Cl_p - Bph)^* \quad (4)$$

$$(Cl_p - Bph)^* \rightarrow Cl_p - Bph + \text{heat} \quad (5)$$

where $Cl_p$–Bph denotes a PCB molecule containing $p$ chlorine atom.

$H^\bullet$ radicals generated from the irradiated hydrocarbons can interact with carbon atoms in C–Cl bonds of PCBs [41], particularly at sites with a low partial charge. Given that the bond dissociation energy of a C–H bond is in a higher range than that of a C–Cl bond [42], the interaction with $H^\bullet$ can lead to the cleavage of the C–Cl bond and subsequent formation of a new C–H bond, as shown in Reaction (6), liberating chloride ions [30].

$$(Cl_p - Bph)^* + H^\cdot \rightarrow Cl_{p-1} - Bph - H + Cl^- \quad (6)$$

A complete sequence of the dechlorination steps is provided in Fig. S1 (Appedix 1) and summarized in abbreviated form in Fig. S2 (Appendix 2) of the ESI material. Based on these results, the proposed mechanism for the dechlorination of PCB 20 under electron beam irradiation is presented in Fig. 1. Notably, this representation reveals that the dechlorination pathway of PCB 20 is similar to that of 1,2,4-trichlorobenzene [19].

### 2.2. Mathematical expressions

#### 2.2.1. Assumptions

To derive the kinetic equations for the radiolytic dechlorination kinetics of PCBs, the following assumptions were adopted: Irradiation was performed using a parallel electron beam, with the distance from the source to the bottom of the sample fixed at 20 cm; under these conditions, variations in source-to-surface distance have a negligible influence on the depth dose distribution [43,44]. The physicochemical properties were assumed to be uniform across each horizontal cross-section of the sample, and the sample temperature was considered constant during each 5-s irradiation interval. Convective and diffusive mass transport within the sample volume was neglected. Given the low concentrations of PCBs and biphenyl, their presence was assumed not to significantly affect the absorbed dose in PCB-free transformer oil. Furthermore, due to their short lifetimes, excited species and radicals were treated as reactive intermediates following the quasi-steady-state approximation.

#### 2.2.2. Depth-dependent concentration of hydrogen radical

In radiolysis, the percentage depth dose (PDD) is a key parameter that describes the variation of absorbed dose with depth in a given medium [45]. PDD is defined as the ratio of the absorbed dose at a specific depth $d$ along the central axis of the beam to the maximum absorbed dose [46], as expressed in Eq. (7).

$$PDD = \frac{D_d}{D_{max}} = \frac{D_s}{D_{max}} \frac{D_d}{D_s} \quad (7)$$

where $D_d$, $D_s$, $D_{max}$ present the absorbed doses at depth $d$, at the sample surface ($d = 0$), and at the depth of maximum dose ($d_{max}$), respectively.

On the other hand, the model for the PDD curve can be corrected by the Mayneord factor [47]. Eq. (8) presents a general relationship between *PDD* and sample depth.

$$PDD = K_s \left(\frac{f_1 + d}{f_2 + d}\right)^2 e^{-\mu d} \quad (8)$$

where $F(d) = K_s((f_1 + d)/(f_2 + d))^2$ represents the Mayneord factor, and the term $e^{-\mu d}$ accounts for the exponential tail of the PDD curve [48]. Here, $K_s$ is the scattering coefficient, while $f_1$, $f_2$, and $\mu$ are constant parameters.

By combining Eqs. (7) and (8), Eq. (9) is obtained.

$$\frac{D_d}{D_s} = K_D \left(\frac{f_1 + d}{f_2 + d}\right)^2 e^{-\mu d} \quad (9)$$

where $K_D = K_s D_{max}/D_s$.

Additionally, the absorbed dose is directly proportional to the dose rate ($E$) and the exposure time ($t$), as described by Eq. $D = Et$ [49]. This relationship allows us to derive Eq. (10).

$$\frac{E_d}{E_s} = \frac{D_d}{D_s} \quad (10)$$

where $E_d$ and $E_s$ represent the dose rates at depth $d$ and at the surface of the sample, respectively.

Reactions (1)–(3) describe the formation of $H^\bullet$ from hydrocarbons under electron beam irradiation. Given the short lifetime of hydrogen radicals [50] and the excess presence of hydrocarbons, the concentration of $H^\bullet$ at a given depth $d$ can be considered independent of exposure time. Therefore, the generation of $H^\bullet$, which is dependent on the dose rate, can be reasonably assumed to reach a quasi-equilibrium state.

The influence of dose rate on radical formation has been well documented in the literature [51–53]. Sultana et al. [54] and Kusumoto et al. [55] reported that radical concentrations increase with rising dose rates in the lower range. However, at higher dose rates, the concentration tends to level off, reaching a plateau [56]. In a study on the radiolysis of cyclohexane, Dyne and Fletcher [57] observed that the radical concentration exhibited approximately a fourth-root dependence on dose rate. Accordingly, we adopted a fourth-root dependence of [H•] on dose rate (Eq. (11)), consistent with prior radiolysis studies.

$$[H^\cdot]_d \propto (E_d)^{1/4} \quad (11)$$

where $[H^\bullet]_d$ is the concentration of $H^\bullet$ at depth $d$.

Therefore, the depth-dependent concentration of $H^\bullet$ can be determined by using Eq. (12).

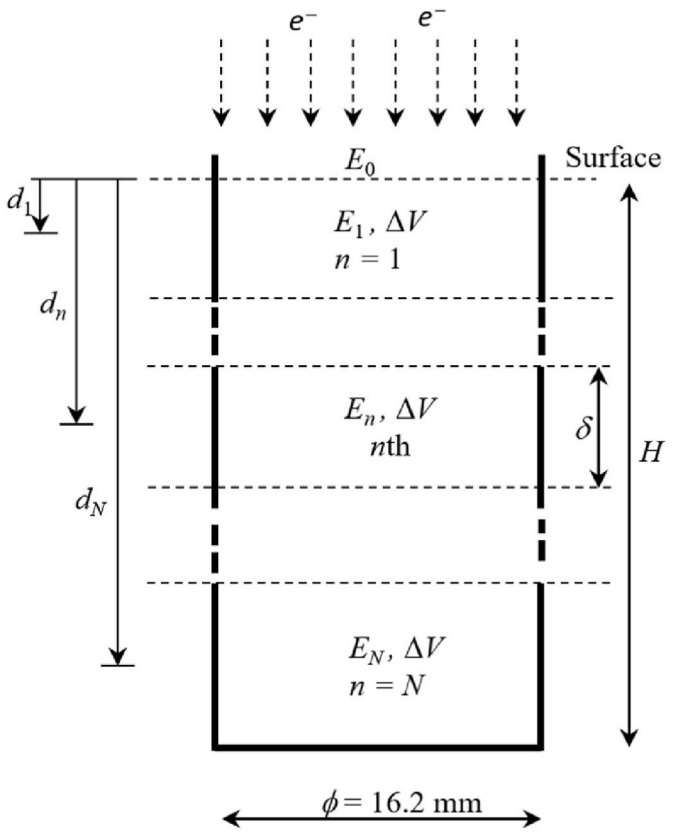


**Fig. 2.** Schematic representation of the sample.

$$\frac{[H^{\cdot}]_d}{[H^{\cdot}]_s} = \left(\frac{E_d}{E_s}\right)^{1/4} \tag{12}$$

where $[H^{\bullet}]_s$ represents the concentration of $H^{\bullet}$ at the surface. Notably, $[H^{\bullet}]_s$ remains constant regardless of changes in sample depth.

### 2.2.3. Time-dependent concentration of PCBs and biphenyl

In radiolysis, radical concentration is dependent on the dose rate [52,58,59] which decreases with increasing sample depth [60]. Consequently, at greater depths within the sample, the concentration of $H^{\bullet}$ is reduced, leading to a lower dechlorination rate of PCBs.

As detailed in Appendix 3 of the ESI material, the time-dependent concentrations of individual PCBs are described by Eqs. (s42-1) to (s42-7), which highlight the influence of $H^{\bullet}$ concentration on the dechlorination kinetics. Given that $H^{\bullet}$ concentration varies with depth, these equations are further modified to include a depth correction factor *F*, resulting in the revised forms shown in Eqs. (s44-1) to (s44-7).

To characterize the depth-dependent concentration of individual PCB, the sample is conceptually discretized into *N* differential volume elements, as illustrated in Fig. 2.

The rate equations (s44-1) to (s44-7) describing PCB dechlorination are applied at various depths along the sample. As illustrated in Fig. 2, each differential volume element can be modeled as a batch reactor. By using Eqs. (s44-1) to (s44-7) to the *n*th differential volume, a system of ordinary differential equations (ODEs), denoted as Eqs. (13)–(1) to (13-7), is obtained.

$$\frac{dx_{1,n}}{dt} = -F_n(k_1 + k_2 + k_3)x_{1,n} \tag{13-1}$$

$$\frac{dx_{2,n}}{dt} = F_n\left(k_1 x_{1,n} - (k_4 + k_5)x_{2,n}\right) \tag{13-2}$$

$$\frac{dx_{3,n}}{dt} = F_n\left(k_2 x_{1,n} - (k_6 + k_7)x_{3,n}\right) \tag{13-3}$$

$$\frac{dx_{4,n}}{dt} = F_n\left(k_3 x_{1,n} - k_8 x_{4,n}\right) \tag{13-4}$$

$$\frac{dx_{5,n}}{dt} = F_n\left(k_4 x_{2,n} + k_6 x_{3,n} - k_9 x_{5,n}\right) \tag{13-5}$$

$$\frac{dx_{6,n}}{dt} = F_n\left(k_5 x_{2,n} + k_7 x_{3,n} + k_8 x_{4,n} - k_{10} x_{6,n}\right) \tag{13-6}$$

$$\frac{dx_{7,n}}{dt} = F_n\left(k_9 x_{5,n} + k_{10} x_{6,n}\right) \tag{13-7}$$

where $F_n$ is the depth correction factor for the *n*th differential volume and $x_{j,n}$ represents the concentration of the *j*th compound in the *n*th differential volume. The index $j = 1$ to 7 corresponds to PCB 20, PCB 5, PCB 6, PCB 11, PCB 1, PCB 2, and biphenyl, respectively, as illustrated in Fig. 1. The terms $k_1$, $k_2$, …, $k_{10}$ denote the effective rate constants for the associated reactions, also defined in Fig. 1.

The solution of the system of ODEs, given by Eqs. (13)–(1) to (13-7), provides the time-dependent concentrations of each compound within the *n*th differential volume. The average concentrations of PCBs and biphenyl across the entire sample are then calculated using Eq. (14).

$$x_j = \frac{1}{V_s}\sum_{n=1}^{N}\left(x_{j,n}\Delta V\right) = \frac{\delta}{d_s}\sum_{n=1}^{N}\left(x_{j,n}\right) \tag{14}$$

where $N = H/\delta$ represents the total number of differential volume elements, *H* is the total sample depth, $\delta$ is the thickness of each differential element, and $V_s$ denotes the total volume of the sample.

### 2.3. Numerical method

PDD parameters ($K_D$, $f_1$, $f_2$, $\mu$) in Eq. (9) were obtained by least-squares fitting (Excel Solver; generalized reduced-gradient) to measured $D_d/D_s$, minimizing SSE (Eq. (15)).

$$SSE = \sum_{m=1}^{M}\left(y_{\text{cal}} - y_{\text{exp}}\right)_m^2 \rightarrow \min \tag{15}$$

where $y_{\text{cal}}$ and $y_{\text{exp}}$ represent the values of $D_d/D_s$ calculated from Eq. (9) and obtained from experimental measurement, and *M* denotes the total number of measurements.

For *n*th differential volume element, the seven-equation ODE system (Eqs. (13-1)–(13-7)) was numerically solved by the fourth-order Runge–Kutta method using initial conditions in Eq. (16).

$$\begin{cases} x_{1,n}(0) = x_{1,0} \\ x_{j,n}(0) = 0 \quad \text{for} \quad j = 2:7 \end{cases} \tag{16}$$

Kinetic constants $k_1$ … $k_{10}$ were estimated by nonlinear least squares (MATLAB, the fmincon function), minimizing Eq. (17) with convergence when successive iterations changed by <5 %.

$$SSE = \sum_{j=1}^{7} SSE_j = \sum_{j=1}^{7}\sum_{i=1}^{4}\left(x_{j,\text{cal}} - x_{j,\text{exp}}\right)_i^2 \rightarrow \min \tag{17}$$

where *j* is the index corresponding to each compound ($j = 1$ to 7, as presented in Fig. 1), and *i* represents the index for the irradiation time intervals ($i = 1$ to 5, corresponding to the exposure time of $t = 0$, 5, 10, 15, and 20 s).

Goodness-of-fit is reported using the coefficient of determination ($R^2$) (Eq. (18)).

$$R_j^2 = 1 - \frac{SSE_j}{TSS_j} \tag{18}$$

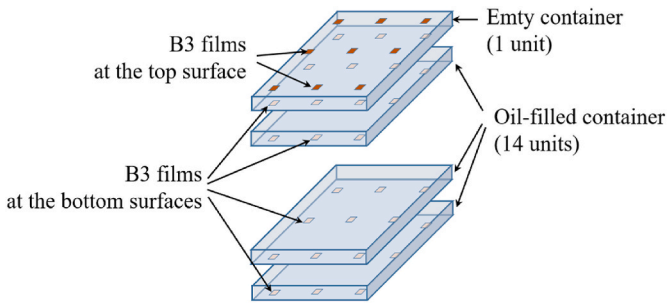


**Fig. 3.** Schematic of the container assembly for depth dose measurement.

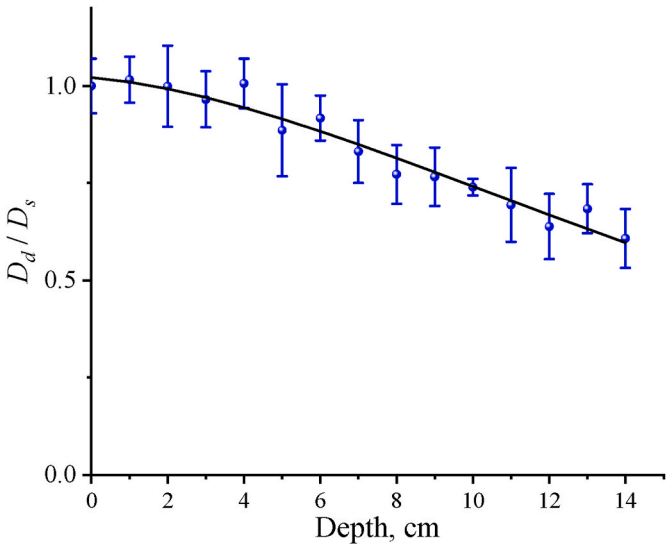


**Fig. 4.** Depth dose curve in PCB-free transformer oil (electron energy of 10 MeV).

**Table 1**
Calculated parameters of depth dose model.

| Parameters | $K_D$ | $f_1$, cm | $f_2$, cm | $\mu$, 1/cm | $R^2$ |
|---|---|---|---|---|---|
| Value | 263.8 | 17.6 | 282.8 | $11.5 \times 10^{-2}$ | 0.957 |

where *TSS* denotes the total sum of squares, determined by Eq. (19).

$$TSS_j = \sum_{i=1}^{5} \left(x_{j,\mathrm{exp}} - \overline{x_{j,\mathrm{exp}}}\right)_i^2 \tag{19}$$

## 3. Experimental

### 3.1. Chemicals and materials

All pure chemicals, 2,3,3′-trichlorobiphenyl (PCB 20), 2,3-dichlorobiphenyl (PCB 5), 2,3′-dichlorobiphenyl (PCB 6), 3,3′-dichlorobiphenyl (PCB 11), 2-chlorobiphenyl (PCB 1), 3-chlorobiphenyl (PCB 2), and biphenyl, each with a purity greater than 99.9 % (w/w), were obtained from LGC Ltd. (UK). Commercial transformer oil, marketed as Transol GIXII with a density of 0.895 g/mL at 20 °C and confirmed to be free of PCBs, was provided by Savita Oil Technologies Ltd. (India). Iso-octane (purity >99.5 % w/w) was purchased from Merck KGaA (Germany).

Individual standard solutions of PCB 20, PCB 5, PCB 6, PCB 11, PCB 1, PCB 2, and biphenyl, each at a concentration of 500 μg/mL in iso-octane, were supplied by CPAChem (Bulgaria).

### 3.2. Measurements of dose

The absorbed dose was measured using B3 radiochromic film (5 × 5 mm), which undergoes a color change upon irradiation with an electron beam. The optical absorbance of the irradiated B3 film at 552 nm, as specified in ISO/ASTM 51310, was measured using a Genesys 20 spectrophotometer and used to construct a calibration curve. During irradiation, the B3 films were positioned perpendicular to the axis of the electron beam. Alanine pellet dosimeters (four pellets per dosimeter), supplied by the Risø High Dose Reference Laboratory, were employed as reference standards for dose verification.

### 3.3. Empirical depth dose determination

A stack of 15 custom-made cubic containers was fabricated from 1.5 mm thick acrylic plastic sheets, each with internal dimensions of 20 × 20 × 1 cm (length × width × height), and arranged vertically, as shown in Fig. 3. The topmost container was left empty and fitted with nine B3 radiochromic films affixed to both its top and bottom surfaces. The remaining 14 containers were filled with PCB-free transformer oil, with each container having nine B3 films attached to its bottom surface.

The absorbed dose of a single acrylic plastic sheet ($d_L$) can be calculated by Eq. (20).

$$d_L = \frac{D_F - D_B}{2} \tag{20}$$

where $D_F$ and $D_B$ represent the absorbed dose at the top and bottom surfaces of the empty container, respectively.

The absorbed dose of the oil at a depth $d$ was calculated using Eq. (21).

$$D_d = D_F - D_n - md_L \tag{21}$$

where $D_n$ is the measured dose at the bottom of $n$th oil-filled container, and $m$ is the number of acrylic plastic sheets traversed by the electron beam.

### 3.4. Irradiation

Pure PCB 20 was diluted in transformer oil to obtain a stock solution with a concentration of 1.438 mmol/L, equivalent to 413.4 mg/kg of PCB 20. Aliquots of 10 and 20 mL of this solution were transferred into glass tubes with an inner radius of 0.81 cm, resulting in sample depths of 5 and 10 cm, respectively. To eliminate dissolved oxygen, nitrogen gas was purged through each sample for 2 min immediately prior to irradiation.

Electron beam irradiation was performed in a top-down, one-sided configuration using a UERL-10-15S2 accelerator with the electron energy of 10 MeV, 1.5 mA. Samples were placed on a conveyor belt and passed through the irradiation chamber. Each exposure lasted 5 s, delivering a dose of 25 kGy. Experimental observations indicated a temperature increase of approximately 2 °C in the samples after each irradiation cycle. To allow the samples to return to their initial temperature, they were held at ambient conditions (25–28 °C) for 10 min between successive irradiations. This process was repeated until the desired cumulative dose was achieved. For each condition, the irradiation was replicated 3 times.

### 3.5. Determination of PCBs concentration

A gas chromatography (GC) equipped with an electron capture detector (ECD) (Model 7890A, Agilent, USA) was used to determine the concentrations of PCBs in the samples. Separation was achieved using a 30 m × 0.25 mm inner diameter fused-silica capillary column coated with a 1 μm film thickness of SE-54 stationary phase. Nitrogen (purity 99.99 %) was used as the carrier gas at a flow rate of 5 mL/min. The

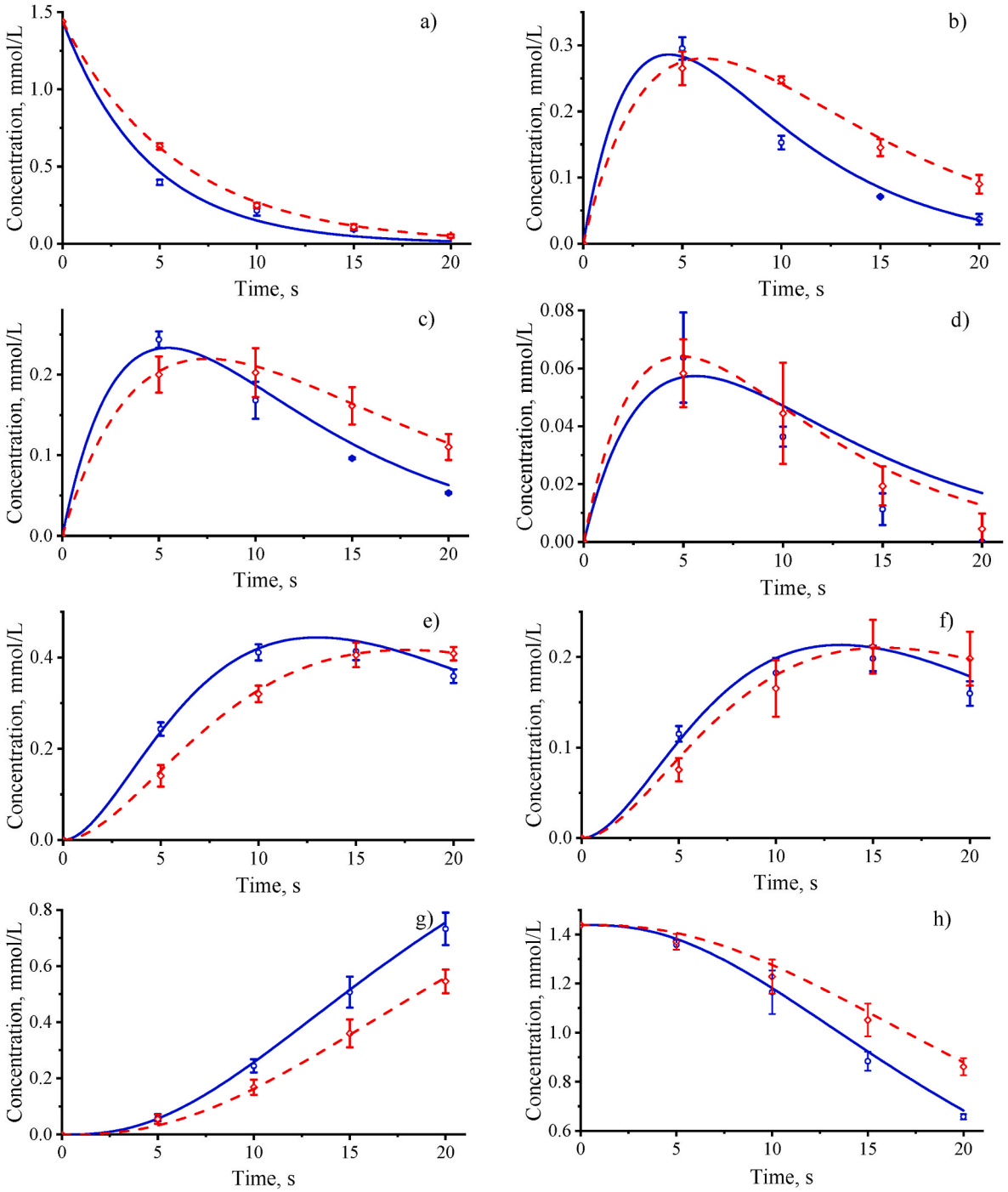


**Fig. 5.** The time-dependent concentration of a) PCB 20, b) PCB 5, c) PCB 6, d) PCB 11, e) PCB 1, f) PCB 2, g) biphenyl, and h) total PCBs in the irradiated sample (blue solid for $H = 5$ cm and red dash for $H = 10$ cm) (electron energy of 10 MeV).

injector and detector temperatures were set at 210 °C and 300 °C, respectively. The oven temperature program consisted of an initial hold at 90 °C for 2 min, followed by a temperature ramp of 15 °C 1/min to 300 °C, and a final hold at 300 °C for 4 min.

PCB analysis was conducted following EPA Victoria Method Number: 6013, employing individual PCB standards in iso-octane (500 μg/mL) supplied by CPAChem Ltd. (Bulgaria). Calibration standards of 5, 10, 20, 30, 50, and 80 μg/mL were prepared by diluting appropriate volumes of the PCB standard solutions in transformer oil. The limit of detection for PCBs was less than 1.5 μg/mL. Calibration was conducted in triplicate, yielding relative standard deviations of 13–24 % at 5 μg/mL and 4–8.5 % at 80 μg/mL.

### 3.6. Simulation of electronic characteristics of PCBs and biphenyl

The molecular structures of the PCBs were optimized by energy minimization using the MM2 force field in Chem3D software, resulting in three-dimensional representations. Based on the optimized geometries, the partial atomic charges and molecular orbitals were calculated using the extended Hückel method.

**Table 2**
Calculated kinetic parameters.

| Reactions | Parameters | Sample depth | |
|---|---|---|---|
| | | $H = 5$ cm | $H = 10$ cm |
| | Rate constant, 1/s | | |
| PCB 20 → PCB 5 | $k_1$ | 0.1284 | 0.0896 |
| PCB 20 → PCB 6 | $k_2$ | 0.0837 | 0.0572 |
| PCB 20 → PCB 11 | $k_3$ | 0.0200 | 0.0256 |
| PCB 5 → PCB 1 | $k_4$ | 0.2428 | 0.1661 |
| PCB 5 → PCB 2 | $k_5$ | 0.0042 | 0.0014 |
| PCB 6 → PCB 1 | $k_6$ | 0.0656 | 0.0757 |
| PCB 6 → PCB 2 | $k_7$ | 0.1464 | 0.1043 |
| PCB 11 → PCB 2 | $k_8$ | 0.0758 | 0.1767 |
| PCB 1 → Bph | $k_9$ | 0.0701 | 0.0526 |
| PCB 2 → Bph | $k_{10}$ | 0.1065 | 0.0989 |
| | Coefficient of determination ($R^2$) | | |
| | PCB 20 | 0.9912 | 0.9996 |
| | PCB 5 | 0.9822 | 0.9930 |
| | PCB 6 | 0.9755 | 0.9962 |
| | PCB 11 | 0.7418 | 0.9421 |
| | PCB 1 | 0.9933 | 0.9985 |
| | PCB 2 | 0.9672 | 0.9881 |
| | Biphenyl | 0.9979 | 0.9962 |
| | Chi-square ($\chi^2$) | | |
| | PCB 20 | $1.45 \times 10^{-1}$ | $2.32 \times 10^{-3}$ |
| | PCB 5 | $6.35 \times 10^{-3}$ | $1.86 \times 10^{-3}$ |
| | PCB 6 | $6.81 \times 10^{-3}$ | $6.13 \times 10^{-4}$ |
| | PCB 11 | $3.14 \times 10^{-2}$ | $7.60 \times 10^{-3}$ |
| | PCB 1 | $2.02 \times 10^{-3}$ | $1.05 \times 10^{-3}$ |
| | PCB 2 | $4.63 \times 10^{-3}$ | $3.12 \times 10^{-3}$ |
| | Biphenyl | $1.72 \times 10^{-3}$ | $1.64 \times 10^{-2}$ |

## 4. Results and discussion

### 4.1. Depth dose distribution in PCB-free transformer oil

It is well established that the efficiency of radiolytic dechlorination of chlorinated compounds is strongly influenced by the absorbed radiation dose [19,25]. However, due to Coulombic interactions and the electron stopping effect [61,62], the dose distribution varies with sample depth, resulting in depth-dependent reaction rates. This spatial variation in dose is a critical factor in accurately modeling the dechlorination kinetics of PCBs.

In this study, the depth dose distribution in PCB-free transformer oil was experimentally measured, and the results are presented in Fig. 4. As illustrated, the absorbed dose decreases with increasing depth. The depth dose curve does not exhibit a pronounced maximum, indicating only a minor skin-sparing effect [63,64]. The therapeutic range of the electron beam, defined as the depth corresponding to 90 % of the surface dose [45], was determined to be 5.5 cm. This value is consistent with previous studies involving paraffin oil [65].

The experimental data demonstrate a strong correlation with the depth dose model described by Eq. (9), as evidenced by the high coefficient of determination ($R^2$) presented in Table 1. Therefore, Eq. (9), along with the fitted parameters provided in Table 1, can be reliably used to predict dose distribution for incorporation into the kinetic modeling of PCB dechlorination.

### 4.2. Kinetic study of the PCBs dechlorination by electron beam irradiation

The radiolytic dechlorination of PCB 20 dissolved in transformer oil was investigated at an initial concentration of 413.4 mg/kg and sample depths of 5 cm and 10 cm. The temporal evolution of PCB and biphenyl concentrations in the irradiated oil is shown by discrete data points in Fig. 5(a)–(g).

As illustrated in Fig. 5(a), the concentration of PCB 20 decreased exponentially with increasing exposure time, which approached zero after 20 s of electron beam irradiation. Shallower sample depths (i.e., 5 cm) led to a more rapid reduction in PCB 20 concentration, confirming the depth dependence of the dechlorination reaction.

Fig. 5(b)–(d) display concentration profiles of dichlorinated biphenyl congeners. These compounds exhibit a characteristic increase followed by a decrease in concentration over time, resulting in well-defined maxima. Notably, increasing the sample depth leads to a temporal shift of these maxima toward longer irradiation times, which is consistent with the reduced reaction rates associated with lower absorbed doses at greater depths [25]. Among the dichlorinated congeners, PCB 5 and PCB 6 were detected at markedly higher concentrations than PCB 11. This observation suggests that *meta*-chlorine dechlorination from PCB 20 is favoured over *ortho*-chlorine dechlorination under the studied conditions.

Within the monochlorinated biphenyl group, PCB 1 consistently exceeds PCB 2 in concentration, as shown in Fig. 5(e) and (f). Both compounds exhibit concentration maxima, with the peak positions shifting to longer irradiation times as the sample depth increases. This indicates the influence of depth dose on the dechlorination kinetics, extending to the intermediate chlorinated species.

As expected, biphenyl, the fully dechlorinated product, was formed in significant quantities, as shown in Fig. 5(g). Its concentration increased steadily with prolonged irradiation, with faster formation observed at shallower depths. After 20 s of electron beam irradiation (corresponding to a dose of approximately 100 kGy) at depths of 5 cm and 10 cm, the total remaining chlorine in PCBs was determined to be 0.845 and 1.166 mmol/L, corresponding to dechlorination efficiencies of 80.4 % and 73.0 %, respectively. These values slightly exceed those reported for γ-radiolytic dechlorination of PCB 54 under comparable conditions [23].

A system of ODEs, presented in Eq. (13), was used to model the dechlorination kinetics. The reaction rate constants obtained from fitting the model to experimental data are listed in Table 2. The simplifying assumptions adopted in the model – constant sample temperature and negligible mass transfer – likely contribute to its limited performance in certain cases. Specifically, (1) the relatively low $R^2$ values for PCB 2 and PCB 11 indicate noticeable deviations between the model predictions and experimental results; and (2) although the influence of sample depth was incorporated through the depth correction factor ($F_n$), which is theoretically independent of the effective rate constants ($k$), the obtained $k$ values exhibited some variation with depth. Further experimental work and model development will be conducted to improve predictive accuracy. Despite these limitations, most fittings yielded high coefficients of determination ($R^2$), demonstrating strong overall agreement between the model and experimental data. Furthermore, the calculated chi-square ($\chi^2$) values for all PCBs were significantly lower than the critical value ($\chi^2 = 9.488$, with 4 degrees of freedom and a significance level of $\alpha = 0.05$), confirming the robustness and reliability of the model in representing the experimental observations.

### 4.3. Correlation between dechlorination kinetics and electronic characteristics

The radiolytic dechlorination of chlorinated organics is controlled mainly by electronic factors, particularly atomic partial charges [66,67] and the distribution of molecular orbitals [68]. Atoms with lower partial charges enhance the likelihood of electron attraction via Coulombic forces, while the presence and spatial configuration of the lowest unoccupied molecular orbitals (LUMOs) can inhibit electron capture [69]. These principles are instrumental in understanding the reactivity of PCBs and biphenyl, as illustrated in Fig. 6 and further detailed in Appendix 4 of the ESI material.

The distribution of partial charges and LUMOs in specific PCB congeners dictates their dechlorination pathways. In PCB 20, the carbon atom at position C(9) exhibits the lowest partial charge and is not surrounded by interfering LUMOs, making it the most reactive site for incoming electrons or $H^{\bullet}$. Consequently, PCB 5 emerges as the dominant

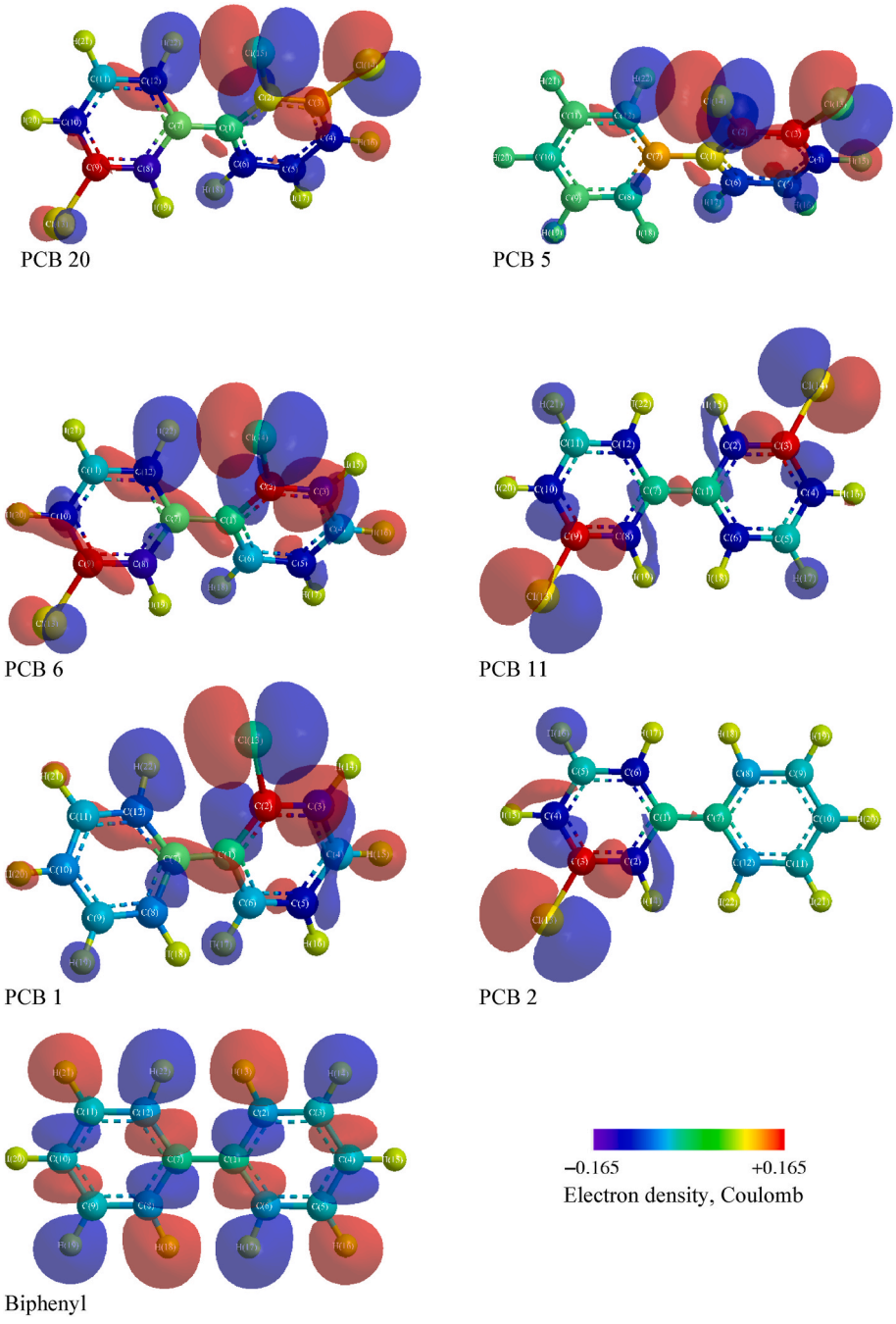


**Fig. 6.** The schematic representation of the partial charge and molecular orbitals in PCBs and biphenyl.

secondary product upon electron irradiation. A similar mechanism operates in PCB 5, where C(3) possesses the lowest partial charge and serves as a potential site for further reaction leading to PCB 1, indicated by $k_4 \gg k_5$ (Table 2). However, overlapping LUMOs from adjacent chlorine atoms obstruct this site, thereby limiting its reactivity and contributing to the observed gradual decline in PCB 5 concentration (Fig. 5(b)).

In PCB 6, both C(2) and C(9) display comparable partial charge magnitudes, yet C(9) is more accessible to electron or $H^{\bullet}$ interaction due to the absence of LUMO overlap. This structural and electronic configuration favors the formation of PCB 1 over PCB 2 during irradiation. Nevertheless, the experimentally determined rate constant $k_6$ was found to be lower than $k_7$, suggesting that factors beyond steric and electronic effects may influence the reaction kinetics. Muthukrishnan et al. [70] reported that, for 2,4-dichlorobiphenyl, the *ortho*-chlorine bond exhibits a lower activation energy for cleavage owing to the planar structure of the resulting products. It is well established that PCB 2 adopts a planar structure, whereas PCB 1 does not [71]. This structural difference may facilitate the preferential dechlorination of PCB 6 to PCB 2.

Comparing PCB 1 and PCB 2, the C(2) atom in PCB 1 has a higher partial charge and is more influenced by neighboring LUMOs than the C (3) atom in PCB 2, potentially explaining the relatively slower dechlorination rate of PCB 1. This is consistent with $k_9 < k_{10}$.

By contrast, biphenyl exhibits a narrow range of partial charges across its planar carbon framework (−0.05 to +0.05 Coulombs) and a delocalized π-electron system arising from overlapping orbitals of single and double bonds. This delocalization promotes energy dispersion and facilitates electron mobility, contributing to the molecule's high

stability under irradiation conditions [72]. Across the series of PCBs examined, *meta*-chlorinated congeners generally show a higher propensity for dechlorination than *ortho*-chlorinated counterparts, a trend that aligns with prior experimental observations [73–75]. However, the distortion of the molecular electronic structure could not be considered using the Hückel method [76]. Future investigations will focus on determining experimental dynamic parameters to enable a more comprehensive analysis of the electronic structure through quantum chemical calculations.

## 5. Conclusions

Electron beam irradiation was applied to dechlorinate PCB 20 in transformer oil, with variations in sample depth and exposure time. PCB 20 underwent stepwise dechlorination to form lower-chlorinated congeners (PCB 5, PCB 6, PCB 11, PCB 1, PCB 2) and biphenyl. The efficiency of chlorine removal decreased with increasing sample depth. For instance, after 20 s of irradiation, the total chlorine atom concentration in PCBs decreased by 80.4 % and 73.0 % relative to the initial value for sample depths of 5 cm and 10 cm, respectively. A kinetic model based on a radical-mediated mechanism was developed, incorporating the effects of the depth dose distribution. This model, comprising a system of seven ordinary differential equations (ODEs), showed good agreement with experimental data and allowed for the estimation of the reaction rate constants along the dechlorination pathway.

Analysis of the electronic properties of the PCBs revealed that the partial atomic charges and molecular orbital distributions influence dechlorination rates. Specifically, C–Cl bonds with a lower partial charge on the carbon atom were more susceptible to cleavage. Conversely, the presence of a LUMO surrounding the carbon atom hindered bond dissociation.

This study offers valuable insights into the kinetics of radiolytic dechlorination of PCBs in transformer oil via electron beam irradiation without the need for additives, establishing a foundation for further optimization and control of electron-beam-based destruction technologies. In future work, kinetics will be developed to account for additional influencing factors, including mass and heat transfer phenomena, temperature variations, the physicochemical properties of the oil matrix, and electron energy. Such investigations will contribute to the practical scaling of the process for industrial applications.

## CRediT authorship contribution statement

**Hoang Trung Thong:** Writing – original draft, Methodology, Investigation, Conceptualization. **Phan Dinh Tuan:** Writing – review & editing, Supervision, Conceptualization. **Hai D. Tran:** Writing – original draft, Investigation. **Phan Dinh Dong:** Visualization. **Dinh Thi Nga:** Visualization. **Trinh Van Tuyen:** Supervision, Conceptualization. **Uyen P.N. Tran:** Writing – review & editing, Investigation. **Mai Thanh Tung:** Methodology. **Dang Van Phu:** Investigation.

## Conflict of interest

The authors declare that there are no conflicts of interest regarding the publication of this paper.

## Acknowledgements

This study received financial support from the Ministry of Science and Technology of Vietnam through the project identified by code ĐTĐLCN.69/22.

## Appendix A. Supplementary data

Supplementary data to this article can be found online at https://doi.org/10.1016/j.jics.2025.102251.

## References

[1] A. Munawar, M.S. Akram, M.T. Javed, M. Shahid, Polychlorinated biphenyls (PCBs): characteristics, toxicity, phytoremediation, and use of transgenic plants for PCBs degradation, in: M. Hasanuzzaman, M.N.V. Prasad (Eds.), Handbook of Bioremediation, Elsevier, 2021, pp. 677–687, https://doi.org/10.1016/B978-0-12-819382-2.00043-0.

[2] L. Montano, C. Pironti, G. Pinto, M. Ricciardi, A. Buono, C. Brogna, M. Venier, M. Piscopo, A. Amoresano, O. Motta, Polychlorinated biphenyls (PCBs) in the environment: occupational and exposure events, effects on human health and fertility, Toxics 10 (7) (2022) 365, https://doi.org/10.3390/toxics10070365.

[3] M.Z. Hashmi, A.F. Mughal, Microbial and chemically induced reductive dechlorination of polychlorinated biphenyls in the environment, Environ. Sci. Pollut. Res. 32 (5) (2025) 2167–2181, https://doi.org/10.1007/s11356-024-35831-0.

[4] J. Falandysz, M. Rose, A.R. Fernandes, Mixed poly-brominated/chlorinated biphenyls (PXBs): widespread food and environmental contaminants, Environ. Int. 44 (2012) 118–127, https://doi.org/10.1016/j.envint.2012.03.006.

[5] M.D. Erickson, R.G. Kaley, Applications of polychlorinated biphenyls, Environ. Sci. Pollut. Res. 18 (2011) 135–151, https://doi.org/10.1007/s11356-010-0392-1.

[6] K. Breivik, A. Sweetman, J.M. Pacyna, K.C. Jones, Towards a global historical emission inventory for selected PCB congeners—a mass balance approach: 1. Global production and consumption, Sci. Total Environ. 290 (1–3) (2002) 181–198, https://doi.org/10.1016/S0048-9697(01)01075-0.

[7] K. Breivik, A. Sweetman, J.M. Pacyna, K.C. Jones, Towards a global historical emission inventory for selected PCB congeners—a mass balance approach: 3. An update, Sci. Total Environ. 377 (2–3) (2007) 296–307, https://doi.org/10.1016/j.scitotenv.2007.02.026.

[8] L. Melymuk, J. Blumenthal, O. Sáňka, A. Shu-Yin, V. Singla, K. Šebková, K. P. Fedinick, M.L. Diamond, Persistent problem: global challenges to managing PCBs, Environ. Sci. Technol. 56 (12) (2022) 9029–9040, https://doi.org/10.1021/acs.est.2c01204.

[9] C. González, D.B. Guerrón, Economic feasibility proposal for treatment and/or disposal technologies of dielectric oils contaminated with PCB, Heliyon 7 (2) (2021) e05838, https://doi.org/10.1016/j.heliyon.2020.e05838.

[10] D.L. Desai, E.J. Anthony, J. Wang, A pilot-plant study for destruction of PCBs in contaminated soils using fluidized bed combustion technology, J. Environ. Manag. 84 (3) (2007) 299–304, https://doi.org/10.1016/j.jenvman.2006.06.006.

[11] H.I. Gomes, C. Dias-Ferreira, A.B. Ribeiro, Overview of in situ and ex situ remediation technologies for PCB-contaminated soils and sediments and obstacles for full-scale application, Sci. Total Environ. 445–446 (2013) 237–260, https://doi.org/10.1016/j.scitotenv.2012.11.098.

[12] R. Jing, S. Fusi, B.V. Kjellerup, Remediation of polychlorinated biphenyls (PCBs) in contaminated soils and sediment: state of knowledge and perspectives, Front. Environ. Sci. 6 (2018) 79, https://doi.org/10.3389/fenvs.2018.00079.

[13] I.-H. Jung, M.-J. Lee, Y.-J. Mah, Decomposition of PCBs in transformer oil using an electron beam accelerator, Radiat. Phys. Chem. 81 (7) (2012) 899–905, https://doi.org/10.1016/j.radphyschem.2011.12.042.

[14] N. Tajima, J. Hasegawa, K. Horioka, An approach to reuse of PCB-contaminated transformer oil using gamma radiolysis: basic decomposition property of PCB and 1,2,4-trichlorobenzene under gamma ray irradiation, J. Nucl. Sci. Technol. 45 (7) (2008) 601–609, https://doi.org/10.1080/18811248.2008.9711458.

[15] M.A. Mousa, J.F. Quensen, K. Chou, S.A. Boyd, Microbial dechlorination alleviates inhibitory effects of PCBs on mouse gamete fertilization *in Vitro*, Environ. Sci. Technol. 30 (6) (1996) 2087–2092, https://doi.org/10.1021/es950929x.

[16] J.F. Brown Jr., H. Feng, D.L. Bedard, M.J. Brennan, J.C. Carnahan, R.J. May, Environmental dechlorination of PCBs, Environ. Toxicol. Chem. 6 (8) (1987) 579–593, https://doi.org/10.1002/etc.5620060802.

[17] Z. Yun, H. Hou, M. Yin, Z. Wu, S. Sun, L. Zhao, F. Fan, Z. Huang, Enhancement of relatively non-toxic dechlorination of PCBs from thermal desorption off-gas over manganese-doped iron-based bimetallic catalyst, Chem. Eng. J. 448 (2022) 137713, https://doi.org/10.1016/j.cej.2022.137713.

[18] V. Múčka, B. Lízalová, M. Pospíšil, R. Silber, D. Poláková, Radiation dechlorination of PCE and TCE in aqueous solutions, Czech. J. Phys. 53 (2003) A383–A389, https://doi.org/10.1007/s10582-003-0048-1.

[19] S. Karimov, E. Abdullayev, M. Millet, M. Gurbanov, Radiolytic degradation of 1, 2, 4-trichlorobenzene (TCB) in some organic solvents by gamma rays: the kinetic properties of complete dechlorination of TCB and its pathway, Heliyon 10 (10) (2024) e31547, https://doi.org/10.1016/j.heliyon.2024.e31547.

[20] V.S. Kosobutskii, Radiation-initiated dechlorination of organochlorine ecotoxicants, High Energy Chem. 42 (2008) 78–82, https://doi.org/10.1134/S0018143908020021.

[21] M. Siwek, T. Edgecock, Application of electron beam water radiolysis for sewage sludge treatment—a review, Environ. Sci. Pollut. Res. 27 (2020) 42424–42448, https://doi.org/10.1007/s11356-020-10643-0.

[22] M. Chaychian, J. Silverman, M. Al-Sheikhly, D.L. Poster, P. Neta, Ionizing radiation induced degradation of tetrachlorobiphenyl in transformer oil, Environ. Sci. Technol. 33 (14) (1999) 2461–2464, https://doi.org/10.1021/es9900914.

[23] M. Chaychian, C. Jones, D. Poster, J. Silverman, P. Neta, R. Huie, M. Al-Sheikhly, Radiolytic dechlorination of polychlorinated biphenyls in transformer oil and in marine sediment, Radiat. Phys. Chem. 65 (4–5) (2002) 473–478, https://doi.org/10.1016/S0969-806X(02)00359-6.

[24] A.T. Fintzou, M.G. Kontominas, A.V. Badeka, M.R. Stahl, K.A. Riganakos, Effect of electron-beam and gamma-irradiation on physicochemical and mechanical properties of polypropylene syringes as a function of irradiation dose: study under

vacuum, Radiat. Phys. Chem. 76 (7) (2007) 1147–1155, https://doi.org/10.1016/j.radphyschem.2006.11.009.
[25] C.G. Jones, J. Silverman, M. Al-Sheikhly, P. Neta, D.L. Poster, Dechlorination of polychlorinated biphenyls in industrial transformer oil by radiolytic and photolytic methods, Environ. Sci. Technol. 37 (24) (2003) 5773–5777, https://doi.org/10.1021/es030412i.
[26] A. Singh, W. Kremers, P. Smalley, G.S. Bennett, Radiolytic dechlorination of polychlorinated biphenyls, Radiat. Phys. Chem. 25 (1–3) (1985) 11–19, https://doi.org/10.1016/0146-5724(85)90244-4.
[27] V. Múčka, R. Silber, M. Kropáček, M. Pospíšil, V. Kliský, Electron beam degradation of polychlorinated biphenyls, Radiat. Phys. Chem. 50 (5) (1997) 503–510, https://doi.org/10.1016/S0969-806X(97)00059-5.
[28] T. Sawai, Y. Shinozaki, Radiolytic dechlorination of polychlorinated biphenyls (PCB) in organic solutions, Chem. Lett. 1 (10) (1972) 865–868, https://doi.org/10.1246/cl.1972.865.
[29] T. Sawai, T. Shimokawa, Y. Shinozaki, The radiolytic-chain dechlorination of polychlorinated biphenyls in alkaline 2-propanol solutions, Bull. Chem. Soc. Jpn. 47 (8) (1974) 1889–1893, https://doi.org/10.1246/bcsj.47.1889.
[30] M. Al-Sheikhly, J. Silverman, P. Neta, L. Karam, Mechanisms of ionizing radiation-induced destruction of 2, 6-dichlorobiphenyl in aqueous solutions, Environ. Sci. Technol. 31 (9) (1997) 2473–2477, https://doi.org/10.1021/es960741t.
[31] A. Singh, W. Kremers, Radiolytic dechlorination of polychlorinated biphenyls using alkaline 2-propanol solutions, Radiat. Phys. Chem. 65 (4–5) (2002) 467–472, https://doi.org/10.1016/S0969-806X(02)00360-2.
[32] M.M. El-Dessouky, Mechanism of organic reactions under the effect of radiolysis, in: Proceedings of the 9th ASAT Conference, 2001, pp. 1255–1274. Cairo, Egypt.
[33] D.C. Schmelling, D.L. Poster, M. Chaychian, P. Neta, J. Silverman, M. Al-Sheikhly, Degradation of polychlorinated biphenyls induced by ionizing radiation in aqueous micellar solutions, Environ. Sci. Technol. 32 (2) (1998) 270–275, https://doi.org/10.1021/es9704601.
[34] A. Bjelić, M. Grilc, B. Likozar, Catalytic hydrogenation and hydrodeoxygenation of lignin-derived model compound eugenol over Ru/C: intrinsic microkinetics and transport phenomena, Chem. Eng. J. 333 (2018) 240–259, https://doi.org/10.1016/j.cej.2017.09.135.
[35] A. Bjelić, M. Grilc, M. Huš, B. Likozar, Hydrogenation and hydrodeoxygenation of aromatic lignin monomers over Cu/C, Ni/C, Pd/C, Pt/C, Rh/C and Ru/C catalysts: mechanisms, reaction micro-kinetic modelling and quantitative structure-activity relationships, Chem. Eng. J. 359 (2019) 305–320, https://doi.org/10.1016/j.cej.2018.11.107.
[36] H.T. Thong, T.D. Hai, D.T. Nga, T.V. Tuyen, P.D. Tuan, Dechlorination of polychlorinated biphenyls in used transformer oil by accelerated electron beam irradiation, J. Indian Chem. Soc. 102 (6) (2025) 101724, https://doi.org/10.1016/j.jics.2025.101724.
[37] H. Mitsui, F. Hosoi, T. Kagiya, γ-radiation-induced cross-linking of polyethylene, Polym. J. 4 (1) (1973) 79–86, https://doi.org/10.1295/polymj.4.79.
[38] H.-J. Deyerl, T. Gilbert, I. Fischer, P. Chen, Kinetics and dynamics in the photodissociation of the allyl radical, J. Chem. Phys. 107 (8) (1997) 3329–3332, https://doi.org/10.1063/1.474704.
[39] E.N. Weber, P.F. Forsyth, R.H. Schuler, Radical production in the radiolysis of the hydrocarbons, Radiat. Res. 3 (1) (1955) 68–76, https://doi.org/10.2307/3570273.
[40] L.B. Harding, Y. Georgievskii, S.J. Klippenstein, Predictive theory for hydrogen atom−hydrocarbon radical association kinetics, J. Phys. Chem. A 109 (21) (2005) 4646–4656, https://doi.org/10.1021/jp0508608.
[41] B.-Z. Wu, H.-Y. Chen, S.J. Wang, C.M. Wai, W. Liao, K. Chiu, Reductive dechlorination for remediation of polychlorinated biphenyls, Chemosphere 88 (7) (2012) 757–768, https://doi.org/10.1016/j.chemosphere.2012.03.056.
[42] W.S. McGivern, A. Derecskei-Kovacs, S.W. North, J.S. Francisco, Computationally efficient methodology to calculate C−H and C−X (X = F, Cl, and Br) bond dissociation energies in haloalkanes, J. Phys. Chem. A 104 (2) (2000) 436–442, https://doi.org/10.1021/jp993275d.
[43] C.B. Saw, K.M. Ayyangar, T. Pawlicki, L.J. Korb, Dose distribution considerations of medium energy electron beams at extended source-to-surface distance, Int. J. Radiat. Oncol. Biol. Phys. 32 (1) (1995) 159–164, https://doi.org/10.1016/0360-3016(94)00598-F.
[44] J.H.L. Mott, N.S. West, Essentials of depth dose calculations for clinical oncologists, Clin. Oncol. 33 (1) (2021) 5–11, https://doi.org/10.1016/j.clon.2020.06.021.
[45] W. Strydom, W. Parker, M. Olivares, Electron beams: physical and clinical aspects, in: E.B. Podgorsak (Ed.), Radiation Oncology Physics: a Handbook for Teachers and Students, International Atomic Energy Agency (IAEA), Vienna, Austria, 2005, pp. 273–299.
[46] A.H. Karimi, I.J. Das, N. Chegeni, I. Jabbari, F. Jafari, G. Geraily, Beam quality and the mystery behind the lower percentage depth dose in grid radiation therapy, Sci. Rep. 14 (2024) 4510, https://doi.org/10.1038/s41598-024-55197-0.
[47] E.B. Podgorsak, External photon beams: physical aspects, in: E.B. Podgorsak (Ed.), Radiation Oncology Physics: a Handbook for Teachers and Students, International Atomic Energy Agency (IAEA), Vienna, Austria, 2005, pp. 161–217.
[48] X.-J. Li, Y.-C. Ye, Y.-S. Zhang, J.-M. Wu, Empirical modeling of the percent depth dose for megavoltage photon beams, PLoS One 17 (1) (2022) e0261042, https://doi.org/10.1371/journal.pone.0261042.
[49] W. Rühm, G.E. Woloschak, R.E. Shore, T.V. Azizova, B. Grosche, O. Niwa, S. Akiba, T. Ono, K. Suzuki, T. Iwasaki, N. Ban, M. Kai, C.H. Clement, S. Bouffler, H. Toma, N. Hamada, Dose and dose-rate effects of ionizing radiation: a discussion in the light of radiological protection, Radiat. Environ. Biophys. 54 (2015) 379–401, https://doi.org/10.1007/s00411-015-0613-6.
[50] S. Jiang, H. Zheng, W. Yan, T. Wang, C. Wang, S. Li, H. Xie, G. Li, X. Zheng, H. Fan, X. Yang, L. Jiang, Capturing hydrogen radicals by neutral metal hydroxides, J. Phys. Chem. Lett. 14 (10) (2023) 2481–2486, https://doi.org/10.1021/acs.jpclett.3c00079.
[51] N.M. Schneider, M.M. Norton, B.J. Mendel, J.M. Grogan, F.M. Ross, H.H. Bau, Electron–water interactions and implications for liquid cell electron microscopy, J. Phys. Chem. C 118 (38) (2014) 22373–22382, https://doi.org/10.1021/jp507400n.
[52] N.L.K. Thiher, S.M. Schissel, J.L.P. Jessop, Influence of monomer structure and dose rate on kinetic elements in electron-beam polymerizations, Radiat. Phys. Chem. 189 (2021) 109737, https://doi.org/10.1016/j.radphyschem.2021.109737.
[53] A. Alanazi, J. Meesungnoen, J.-P. Jay-Gerin, Linear energy transfer dependence of transient yields in water irradiated by 150 keV–500 MeV protons in the limit of low dose rates, Can. J. Chem. 98 (8) (2020) 427–433, https://doi.org/10.1139/cjc-2020-0113.
[54] A. Sultana, J. Meesungnoen, J.-P. Jay-Gerin, High-dose-rate effects in the radiolysis of water at elevated temperatures, Can. J. Chem. 99 (7) (2021) 594–602, https://doi.org/10.1139/cjc-2021-0012.
[55] T. Kusumoto, A. Danvin, T. Mamiya, A. Arnone, S. Chefson, C. Galindo, P. Peaupardin, Q. Raffy, N. Kamiguchi, D. Amano, K. Sasai, T. Konishi, S. Kodaira, Dose rate effects on hydrated electrons, hydrogen peroxide, and a OH radical molecular probe under clinical energy protons, Radiat. Res. 201 (4) (2024) 287–293, https://doi.org/10.1667/RADE-23-00244.1.
[56] G. Blain, J. Vandenborre, D. Villoing, V. Fiegel, G.R. Fois, F. Haddad, C. Koumeir, L. Maigne, V. Métivier, F. Poirier, V. Potiron, S. Supiot, N. Servagent, G. Delpon, S. Chiavassa, Proton irradiations at ultra-high dose rate vs. conventional dose rate: strong impact on hydrogen peroxide yield, Radiat. Res. 198 (3) (2022) 318–324, https://doi.org/10.1667/RADE-22-00021.1.
[57] P.J. Dyne, J.W. Fletcher, Radiation chemistry of cyclohexane: II. Dose rate effects on the formation and destruction of cyclohexene, Can. J. Chem. 38 (6) (1960) 851–857, https://doi.org/10.1139/v60-122.
[58] J.J.T. Bosch, R. Braams, Dependence of the G value for radical production on the physical state, Radiat. Res. 36 (3) (1968) 544–554, https://doi.org/10.2307/3572587.
[59] R. Labarbe, L. Hotoiu, J. Barbier, V. Favaudon, A physicochemical model of reaction kinetics supports peroxyl radical recombination as the main determinant of the FLASH effect, Radiother. Oncol. 153 (2020) 303–310, https://doi.org/10.1016/j.radonc.2020.06.001.
[60] D. Jurado, T. Eudaldo, P. Carrasco, N. Jornet, A. Ruiz, M. Ribas, Pantak Therapax SXT 150: performance assessment and dose determination using IAEA TRS-398 protocol, Br. J. Radiol. 78 (932) (2005) 721–732, https://doi.org/10.1259/bjr/15782649.
[61] J.H.L. Mott, J.M. Daniel, Interactions of electromagnetic radiation and subatomic particles with matter – part 2, Clin. Oncol. 33 (7) (2021) 455–460, https://doi.org/10.1016/j.clon.2021.02.005.
[62] M. Usta, M.Ç. Tufan, G. Aydın, A. Bozkurt, Stopping power and dose calculations with analytical and Monte Carlo methods for protons and prompt gamma range verification, Nucl. Instrum. Methods Phys. Res. A. 897 (2018) 106–113, https://doi.org/10.1016/j.nima.2018.04.045.
[63] C.H. Hahn, I.G. Kim, S.T. Park, W.J. Kim, B.S. Moon, D.S. Yoo, S.Y. Ha, B.J. Ahn, Y. J. Ha, C.Y. Jung, S.H. Jung, B.H. Cho, B.C. Lee, Y.H. Han, C.E. Chung, J. Li, A. P. White, J. Yu, First observation of signals due to KAERI's 10 MeV electron beam by using GEM detectors, J. Kor. Phys. Soc. 50 (4) (2007) 961–976, https://doi.org/10.3938/jkps.50.961.
[64] M.J. Butson, T. Cheung, P. Yu, P. Metcalfe, Effects on skin dose from unwanted air gaps under bolus in photon beam radiotherapy, Radiat. Meas. 32 (3) (2000) 201–204, https://doi.org/10.1016/S1350-4487(99)00276-0.
[65] G. Sekartaji, S. Aisyah, C. Carina, T. Nazara, A. Nainggolan, Comparison of dosimetry characteristics from some bolus materials for 6 and 10 MV photons beam radiation therapy. The 3rd Annual Scientific Meeting on Medical Physics and Biophysics (PIT-FMB) and the 17th South East Asian Congress of Medical Physics (SEACOMP), IOP Publishing, Indonesia, 2020 012028.
[66] S.-H. Lee, B.-D. Lee, Elucidation of the dechlorination pathway of 1, 2, 3, 4-TCDD through atomic charge calculation, Desalination Water Treat. 54 (4–5) (2015) 1421–1425, https://doi.org/10.1080/19443994.2014.899523.
[67] F.-C. Chang, T.-C. Chiu, J.-H. Yen, Y.-S. Wang, Dechlorination pathways of *ortho*-substituted PCBs by UV irradiation in *n*-hexane and their correlation to the charge distribution on carbon atom, Chemosphere 51 (8) (2003) 775–784, https://doi.org/10.1016/S0045-6535(03)00003-1.
[68] R. Daily, D. Minakata, Reactivities of hydrated electrons with organic compounds in aqueous-phase advanced reduction processes, Environ. Sci.: Water Res. Technol. 8 (3) (2022) 543–574, https://doi.org/10.1039/D1EW00897H.
[69] F.H.A. Nasir, K.L. Woon, Charge carrier trapping in organic semiconductors: origins, impact and strategies for mitigation, Synth. Met. 307 (2024) 117661, https://doi.org/10.1016/j.synthmet.2024.117661.
[70] A. Muthukrishnan, M.V. Sangaranarayanan, V.P. Boyarskiy, I.A. Boyarskaya, Regioselective electrochemical reduction of 2,4-dichlorobiphenyl – distinct standard reduction potentials for carbon–chlorine bonds using convolution potential sweep voltammetry, Chem. Phys. Lett. 490 (4–6) (2010) 148–153, https://doi.org/10.1016/j.cplett.2010.03.042.
[71] D. Pan, D.L. Phillips, Investigation of the effects of substitution position on the radical anions of chlorobiphenyls, Chem. Phys. Lett. 318 (1–3) (2000), https://doi.org/10.1016/S0009-2614(00)00025-7, 214-121.
[72] P. Puschnig, C. Ambrosch-Draxl, Density-functional study for the oligomers of poly (*Para*-phenylene): band structures and dielectric tensors, Phys. Rev. B 60 (11) (1999) 7891–7898, https://doi.org/10.1103/PhysRevB.60.7891.

[73] F. Lépine, R. Massé, Degradation pathways of PCB upon gamma irradiation, Environ. Health Perspect. 89 (1990) 183–187, https://doi.org/10.1289/ehp.89-15677.
[74] Y. Wang, X. Si, Y. Si, Dechlorination of 3,3′,4,4′-tetrachlorobiphenyl in aqueous solution by hybrid $Fe^0/Fe_3O_4$ nanoparticle system, J. Exp. Nanosci. 10 (15) (2015) 1166–1179, https://doi.org/10.1080/17458080.2014.986228.
[75] L.O. Ruzo, M.J. Zabik, R.D. Schuetz, Polychlorinated biphenyls: photolysis of 3,4,3′,4′-tetrachlorobiphenyl and 4,4′-dichlorobiphenyl in solution, Bull. Environ. Contam. Toxicol. 8 (1972) 217–218, https://doi.org/10.1007/BF01839515.
[76] W. Kutzelnigg, What I like about hückel theory, J. Comput. Chem. 28 (1) (2007) 25–34, https://doi.org/10.1002/jcc.20470.